Controlling the Luminescence of Carboxyl-Functionalized CdSe/ZnS Core–Shell Quantum Dots in Solution by Binding with Gold Nanorods

ARTICLE *in* THE JOURNAL OF PHYSICAL CHEMISTRY C · OCTOBER 2014

Impact Factor: 4.77 · DOI: 10.1021/jp501281v

4 AUTHORS, INCLUDING:

Monica Iosin
Babeş-Bolyai University
32 PUBLICATIONS **422** CITATIONS
SEE PROFILE

Ana Maria Gabudean
Interdisciplinary research institute on bio-nan…
23 PUBLICATIONS **325** CITATIONS
SEE PROFILE

Simion Astilean
Babeş-Bolyai University
169 PUBLICATIONS **2,543** CITATIONS
SEE PROFILE

THE JOURNAL OF PHYSICAL CHEMISTRY C

Article

pubs.acs.org/JPCC

Controlling the Luminescence of Carboxyl-Functionalized CdSe/ZnS Core−Shell Quantum Dots in Solution by Binding with Gold Nanorods

Monica Focsan,[†] Ana M. Gabudean,[†] Adriana Vulpoi,[‡] and Simion Astilean*,[†]

[†]Nanobiophotonics and Laser Microspectroscopy Center, and [‡]Nanostructured Materials and Bio-Nano-Interfaces Center, Interdisciplinary Research Institute in Bio-Nano-Sciences and Faculty of Physics, Babes-Bolyai University, 1 M. Kogalniceanu, 400084, Cluj-Napoca, Romania

Supporting Information

ABSTRACT: Plasmonic nanostructures offer promising routes toward artificial control of the photoluminescence properties of various emitters. Here, we investigated the photoluminescence of carboxyl-functionalized CdSe/ZnS core−shell quantum dots (c-QDs) localized near gold nanorods (AuNRs) as a function of c-QDs−AuNRs distance using the cetyltrimethylammonium bromide (CTAB) surfactant and Bovine Serum Albumin (BSA) protein layers over coating metal surface as spacer. The direct binding of negatively charged c-QDs to positively charged CTAB (3−4 nm thickness) caused close contact with the metal, resulting in an efficient metal-induced energy transfer (quenching). We found that quenching is modulated by the degree of spectral overlap between the photoluminescence band of c-QDs (620 nm) and longitudinal localized surface plasmon resonance (LSPR) of AuNRs (637 and 733 nm). Deposition of BSA layer over CTAB coated-AuNRs and subsequent decoration with c-QDs yielded an increase in photoluminescence signal when exciting in resonance with the transverse LSPR of AuNRs. On the basis of experimental studies using steady-state and time-resolved fluorescence measurements as well as finite-difference time-domain calculations, we report over 70% quenching efficiency for all investigated AuNRs along with a 4.6-fold in photoluminescence enhancement relative to free c-QDs (39-fold enhancement relative to c-QDs loaded AuNRs) after BSA deposition.

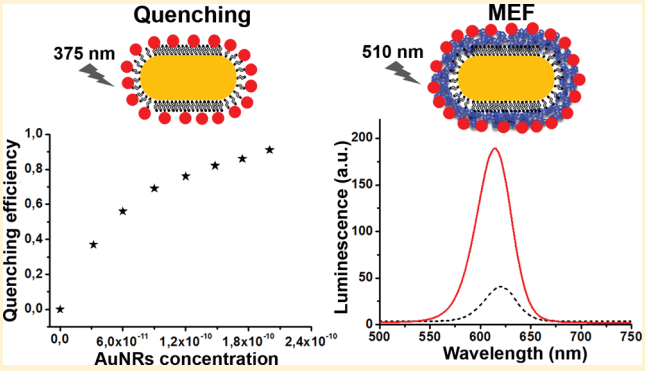

INTRODUCTION

In the field of nanomaterials research, a key goal is to integrate within the same nanosystem multiple functionalities in view of biosensing and bioimaging applications.[1] Resonant coupling between luminescent semiconductor nanoparticles (quantum dots, QDs) and plasmonic metallic nanoparticles can generate new remarkable optical effects, extending thus the applications field of as-designed nanometer-scale hybrid structures. Because of their broad excitation spectra, size-tunable photoluminescence emission spectra, and superior photostability against photobleaching, QDs are very appealing in practical biological applications, especially for multiplexed labeling or multiple immunoassays, as an alternative to ionic and molecular fluorophores.[2] On the other hand, due to their unique optical properties related to their localized surface plasmon resonance (LSPR), gold nanoparticles (AuNPs) act as powerful nanoscale optical antennas,[3] as they are able to significantly enhance light absorption or alter the radiative and nonradiative decay rates of nearby located dipoles.[4] In particular, luminescence enhancement occurs when the dominant relaxation pathway is radiative decay, and vice versa, the luminescence is quenched when the nonradiative decay represents the dominant mechanism. For instance, QDs were successfully exploited for metal-enhanced fluorescence (MEF),[5,6] as well as for fluorescence resonance energy transfer.[1,7]

Furthermore, it has been already demonstrated that several factors influence the plasmon−exciton interaction such as distance between QDs and metal surface, the excitation wavelength, the polarization of excitation, the size of QDs, the geometry of nanoparticles, and the spectral overlap between the luminescence of QDs and the LSPR band of metal nanoparticles.[8−10] The interplay between these factors determines the magnitude of the luminescence enhancement or quenching of QDs. In fact, to control these above-mentioned parameters, a number of experimental methods have been developed, including layer-by-layer (LBL) polyelectrolyte deposition technique,[11] the utilization of hybrid metal@silica@QDs structures,[12] or the utilization of biomolecules (e.g., DNA molecule, streptavidin, biotin) to adjust the interparticle distance.[13−15] However, despite several exper-

Received: February 5, 2014
Revised: October 1, 2014
Published: October 1, 2014

   dx.doi.org/10.1021/jp501281v | J. Phys. Chem. C 2014, 118, 25190−25199

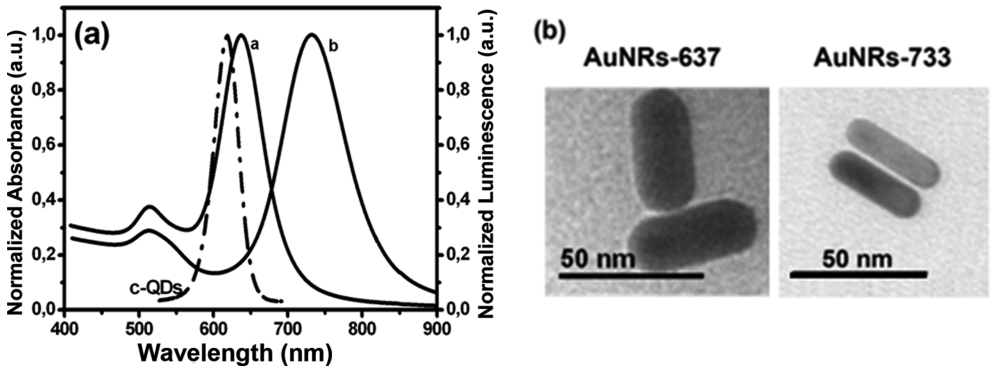

Figure 1. (a) Spectral overlap between the normalized luminescence of c-QDs (dot−dashed spectrum) and the extinction spectra of synthesized AuNRs-637 (spectrum a) and AuNRs-733 (spectrum b), respectively; (b) representative TEM images of the synthesized AuNRs.

imental and theoretical studies performed on solid substrates, MEF of QDs in aqueous solution has received less attention, especially using gold nanorods (AuNRs) as sensitive amplification platform. This interest is essential for a clear understanding of the plasmon−exciton interaction in such QDs@AuNPs hybrid assemblies in aqueous solution, opening thus the door to single molecule detection in biosciences[16] as well as photonic plasmonic devices and solar energy harvesting.[17,18]

Among various shapes of AuNPs, the nanorods are particularly attractive due to the fine-tunability of their plasmon resonances across a wide spectral region, offering thus excellent controllable overlap with the emission of QDs, a key aspect for further multiplexed biodetection applications. While gold nanospheres present a well-defined plasmonic band in the visible spectral region, AuNRs represent a unique class of metallic nanostructures with two surface plasmonic resonances in the visible/near-infrared spectral range associated with oscillations of free electrons along the transverse and longitudinal dimensions of the nanoparticles.[19] Furthermore, due to their strong scattering and local-field enhancements associated with the LSPR excitation at the surface of the nanoparticle, AuNRs are an excellent candidate for the investigation of the luminescence enhancement mechanism.[3]

In this Article, we study the modification of carboxyl-functionalized CdSe/ZnS QDs (c-QDs) luminescence at 620 nm in close vicinity of AuNRs in aqueous solution, as a function of both the spectral overlap between the luminescence of c-QDs and LSPR band of nanoparticles and the interparticle distance. In particular, two types of AuNRs were synthesized utilizing the seed-mediated growth method to exhibit longitudinal LSPR bands at 637 nm (AuNRs-637) and 733 nm (AuNRs-733), respectively. First, we found that the direct interaction between the negatively charged c-QDs with the positively charged cetyltrimethylammonium bromide (CTAB) bilayer that covers AuNRs surface induces a strong luminescence quenching of c-QDs with different efficiency rate, ranging from 78% for AuNRs-733 to 91% for AuNPs-637, and a significant shortening of the exciton lifetime. The highest quenching efficiency obtained for AuNPs-637 (herein 91%) is due to better spectral overlap of the longitudinal LSPR band with the luminescence band of c-QDs. Subsequently, with the aim to increase the spacer thickness, which will directly prevent the quenching mechanism, the surface of CTAB-coated AuNRs-637 was first coated with Bovine Serum Albumin (BSA) protein and then decorated with c-QDs. BSA, a large multidomain protein in plasma with an important role in physiological functions,[20] was selected in this study considering its ability to easily attach to the surface of AuNRs through electrostatic interaction with the positively CTAB bilayer.[21−23] The experimental optical data obtained on the attachment of c-QDs and BSA molecules to the CTAB coated-AuNRs-637 surface were confirmed by simulations based on finite-difference time-domain (FDTD). As a consequence of the increased spacer thickness, the plasmonic enhancement effect became dominant in our hybrid system made of AuNR-637, BSA, and c-QDs, leading to 4.6-fold luminescence enhancement relative to free c-QDs and 39-fold luminescence enhancement relative to the corresponding case of c-QDs@AuNR system, with only slight shortening of the exciton lifetime.

EXPERIMENTAL METHODS

Reagents. Tetrachloroauric (III) acid, cetyltrimethylammonium bromide (CTAB), and ascorbic acid were purchased from Aldrich. Sodium borohydride ($NaBH_4$, 99%) and silver nitrate ($AgNO_3$) were obtained from Merck. Bovine Serum Albumin (BSA, 66 kDa) was purchased from Aldrich. Commercial core/shell CdSe/ZnS quantum dots (c-QDs) with a polyethylene glycol (PEG) surface coating coupled to carboxyl terminal groups were purchased from Evident Technologies Inc. (T2-MPEviTags). The concentration of c-QDs was 12 nmol/mL. All chemicals were used as received.

Samples Preparation. AuNRs of two different aspect ratios were synthesized utilizing the seed-mediated growth method.[19] Gold seeds were first prepared by mixing 1.25 mL of 5 mM $HAuCl_4$, 1.25 mL of 0.2 M CTAB, and 0.9 mL of freshly prepared ice cold 1 mM $NaBH_4$ solution under continuous stirring, resulting in a brownish yellow solution. The growth solution was obtained by mixing 5 mL of 1 mM $HAuCl_4$ with 5 mL of 0.2 M CTAB and various amounts of 4 mM $AgNO_3$. 0.07 mL of 0.0788 M ascorbic acid was then added while gently stirring. Ascorbic acid acts as a mild reducing agent and changes the color of growth solution from dark yellow to colorless. Finally, 0.012 mL of seed solution was added into the as-prepared solution to start the growth of nanorods. The color of the solution gradually changed in the first 15−20 min before finally stabilizing. The obtained AuNRs were collected twice by centrifugation to remove the excess CTAB surfactant and then dispersed in ultrapure water. Considering their longitudinal LSPR peak values at 637 and 733 nm, the as-prepared AuNRs in aqueous solution will be further referred to as AuNRs-637 and AuNRs-733, respectively (see Figure 1, spectra a,b).

dx.doi.org/10.1021/jp501281v | J. Phys. Chem. C 2014, 118, 25190−25199

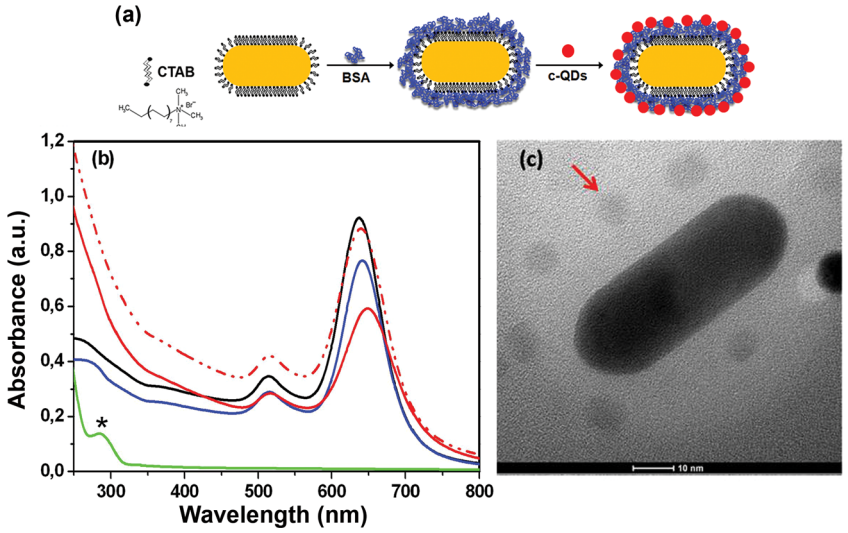

Figure 2. (a) Schematic diagram illustrating the decoration of BSA@AuNRs with c-QDs; (b) extinction spectra of AuNRs-637 (black spectrum), BSA@AuNRs-637 (blue spectrum), and c-QDs decorated BSA@AuNRs-637 (red spectrum), c-QDs@AuNRs-637 (dash−dotted spectrum), and absorption spectrum of free BSA solution (green spectrum); and (c) TEM image of c-QDs decorated BSA@AuNRs-637 corresponding to the red spectrum in (b). Final concentrations of c-QDs and AuNRs-637 are 4×10^{-9} and 10^{-10} M, respectively; red arrow indicates the c-QDs.

The c-QDs are negatively charged (−23.8 mV, zeta-deviation = 0.3 at pH 7.6) in the PBS solution because of the carboxyl-functionalized groups surrounding the surface of the QDs, while the as-prepared AuNRs are positively charged due to the CTAB bilayer adsorbed on the surface of the nanorods (+ 40 mV, zeta-deviation = 8). Therefore, when 2 nM c-QDs in phosphoric buffered saline (PBS, pH 7.6) are mixed with different concentrations of the CTAB-coated AuNRs-637 (stock concentration 1.47×10^{-9} M, as calculated from the absorbance of longitudinal plasmon resonance for a molar extinction coefficient of $\varepsilon = 3.13 \times 10^{9}$ M^{-1} cm^{-1}[24]) and CTAB-coated AuNRs-733 (1.66×10^{-9} M, as calculated from the absorbance of longitudinal plasmon resonance for a molar extinction coefficient of $\varepsilon = 3.6 \times 10^{9}$ M^{-1} cm^{-1}[24]), the c-QDs interacted with AuNRs due to electrostatic interaction.

The attachment of BSA protein to CTAB-coated AuNRs-637 and the subsequent decoration with c-QD was performed in two steps at pH ≈ 7.5. First, the albumin solution was freshly prepared at room temperature by dissolving 1 mg of the solid BSA in 1 mL of ultrapure water at pH 4.7. Next, BSA@AuNRs-637 conjugates were prepared through electrostatic attractive interactions.[21] BSA@AuNRs-637 system was centrifuged at 8000 rpm for 10 min to remove the excess protein in the solution. Second, the c-QDs decorated BSA@AuNRs-637 were obtained by mixing the c-QDs (0.5 mL) and the BSA@AuNRs-637 conjugates (1 mL) for more than 3 h. The final solution was centrifuged to remove the unadsorbed c-QDs, and the obtained c-QDs decorated BSA@AuNRs-637 were redispersed in PBS.

Experimental Measurements. The UV−vis−NIR absorption spectra were measured at room temperature using a Jasco V-670 UV−vis−NIR spectrophotometer with a bandwidth of 2 and 1 nm spectral resolution.

Morphology and mean size of AuNRs were determined by JEOL 100 U type transmission electron microscopy (TEM) operated at 100 kV accelerating voltage in which samples were deposited on carbon-coated copper grids and dried at room temperature. The decoration of BSA@AuNRs-637 conjugates with c-QDs was further confirmed by TEM images using a Tecnai F20 field emission operated at 200 kV accelerating voltage and equipped with an Eagle 4 k CCD camera.

The ζ-potential of the colloidal solutions was measured using a particle analyzer (Nano ZS90 Zetasizer, Malvern Instruments) equipped with a He−Ne laser (633 nm, 5 mW) and using a measurement angle of 90°. Each sample was measured three times, and the mean value was reported.

Luminescence spectra were collected at room temperature using a Jasco LP-6500 spectrofluorimeter equipped with a xenon lamp as a light source. Luminescence quenching experiments were carried out in aqueous solution using an excitation wavelength fixed at 375 nm. Luminescence spectra were recorded in the wavelength range of 560−680 nm. Luminescence quenching was analyzed with values of integrated intensities computed over full spectral range of luminescence bands for both free c-QDs and c-QDs in the presence of increasing AuNRs concentration. For MEF experiments, we used the 510 nm excitation wavelength with bandwidths of 1 nm in excitation and 3 nm in emission. Luminescence measurements were also performed to evaluate the long-term stability of c-QDs in PBS solution.

Fluorescence lifetime measurements were performed on a PicoQuant MicroTime 200 time-resolved confocal fluorescence microscope system (Picoquant GmbH, Germany) based on an inverted microscope (IX 71, Olympus) equipped with a UPLSAPO 60×/NA = 1.2 water immersion objective. The excitation beam was provided by 0.55 μW picosecond diode laser heads (LDH-D-C-375 and LDH-D-C-510, PicoQuant) operating at 375 and 510 nm and pulsed at 20 MHz repetition rate. The samples were dropped on microscope cover glasses and analyzed in solution. The signal collected through the objective was spatially and spectrally filtered by a 50 μm pinhole and long pass emission filters (HQ405LP and HQ519LP, Chroma, Brattleboro, U.S.), respectively, before being focused on a photon counting detector module (PDM-series) Single Photon Avalanche Diode (SPAD) from Micro Photon Devices (MPD). The detector signals were processed by the PicoHarp 300 Time-Correlated Single Photon Counting (TCSPC) data acquisition unit, from PicoQuant. Time-

dx.doi.org/10.1021/jp501281v | J. Phys. Chem. C 2014, 118, 25190−25199

resolved fluorescence decay curves were recorded and analyzed using the SymPhoTime software (version 1.6) provided by PicoQuant. The fluorescence lifetimes were obtained through nonlinear iterative deconvolution algorithm. The instrument response function (IRF) was recorded from the laser light back scattered from plain cover glass working in similar experimental conditions (see Supporting Information Figure S1 for IRF of laser 510 nm). The quality of the fits was judged by analyzing the chi-square (χ^2) values and the distribution of the residuals.

RESULTS AND DISCUSSION

Conjugation of c-QDs to AuNRs. Figure 1a illustrates the spectral relationship between the normalized extinction spectra of two as-synthesized AuNRs (solid spectra) and the luminescence spectrum of c-QDs (dot−dashed spectrum). The almost unmodified spectral position of transverse LSPR band at approximately 514 nm and the longitudinal LSPR bands at 637 and 733 nm (see Figure 1a, spectra a,b) correspond to AuNRs with aspect ratios of ∼2.1 (length/width: 47 ± 4/22 ± 2 nm) and ∼3.2 (length/width: 38 ± 3/12 ± 1 nm), respectively, obtained from analysis of TEM measurements (see Figure 1b for representative images).

Note here that the luminescence emission band of the c-QDs (620 nm) exhibits good spectral overlap with the longitudinal LSPR band of the AuNRs-637 and almost no overlap with the longitudinal LSPR band of AuNRs-733. First, we were interested in examining the luminescence quenching of c-QDs when they are directly conjugated to CTAB-coated AuNRs with two distinct longitudinal LSPR bands (i.e., 637 and 733 nm) and to investigate the involved quenching mechanism. Second, to control the distance between the c-QDs and the AuNRs surface and avoid quenching, a layer of BSA protein was deposited onto the surface of CTAB-coated AuNRs before attaching c-QDs as shown schematically in Figure 2a and proved by TEM analysis in Figure 2c.

The changes of the LSPR spectrum of AuNRs-637 after conjugation with c-QDs and BSA protein were first investigated. The synthesized AuNRs-637 exhibit in solution a weak transverse LSPR band at 514 nm and a strong longitudinal LSPR band at 637 nm (see Figure 2b, black spectrum). The conjugation of CTAB-coated AuNRs with c-QDs (denoted as c-QDs@AuNPs-637) and BSA protein (denoted as BSA@AuNRs-637), respectively, is clearly proven by the modification induced in the longitudinal and transverse LSPR bands, the red-shifts of 3 and 1 nm in the first case (Figure 2b, dash−dotted spectrum) and 4 and 1 nm, respectively, in the second case (Figure 2b, blue spectrum). Such spectral modifications are commonly observed in the case of LSPR sensors[25] and can be assigned to the increase of the local refractive index relative to water. Thus, LSPR results prove the direct attachment of negatively charged c-QDs over the entire surface of positively charged CTAB bilayer wrapped around AuNRs-637 through electrostatic interaction. Additionally, the adsorption of BSA molecules onto the surface of CTAB-coated AuNRs-637 is also confirmed by the sensitive blue-shift of the characteristic absorption band of free BSA in solution from 285 nm, marked with an asterisk in Figure 2b, green spectrum, due to $\pi \rightarrow \pi^*$ transition of the aromatic amino acids residues,[26] to 276 nm. This is clearly indicating the formation of bioconjugates (see Figure 2b, blue spectrum). The adsorption of albumin on the surface of AuNRs-637 could lead to a partial unfolding of protein, causing conformational changes.[27]

Subsequently, more noticeable spectral modifications occur when negatively c-QDs interact with BSA@AuNRs-637 system. Figure 2b, red spectrum, depicts the extinction spectrum of BSA@AuNRs-637 after conjugation with c-QDs. Specifically, red-shifts of the longitudinal and transverse LSPR bands with 7 and 1 nm, respectively, were clearly identified, along with their broadening, indicating the presence of the c-QDs "corona" over the entire surface of the BSA@AuNRs-637 system. Furthermore, the presence of the c-QDs "corona" over the surface of the BSA@AuNRs system was clearly confirmed by TEM (see in Figure 2c; additional TEM images in Supporting Information Figure S2). The LSPR measurements were simulated through FDTD calculations on a single CTAB-coated AuNR, plain BSA-capped AuNR and decorated with c-QDs, using a commercially available FDTD solution software package from Lumerical Solutions, Inc. (Vancouver, Canada).[28] We considered a total field scattered field (TFSF) source with a wave vector k normal to the plan comprising the longitudinal axis of the nanorod and the incident electromagnetic field E_0 polarized along the longitudinal axis. The computation volume was divided into two different regions, one including both incident and scattered fields (total field) while the other including only the scattered field. The extinction spectra were calculated using a 0.8 nm grid size. The nanoparticle was treated as a semispherical end-capped cylinder with 47 nm length and 22 nm width, according to the average size obtained from TEM measurements and the position of the plasmon resonances band at 637 nm. The structure was placed in an aqueous surrounding media (n = 1.33). The dielectric dispersion of gold was determined by best fitting the experimental data reported in the literature.[29] Considering that the CTAB layer is more densely packed on the lateral facets of AuNR as compared to its ends, the coating CTAB shell was modeled as a 4 nm layer with a refractive index of 1.435[30] wrapped around the cylinder, while for less densely packed layer from the ends we considered an effective refractive index of 1.363 obtained for a combination of 30% CTAB and 70% water. Furthermore, the compact layer of BSA covering the AuNR surface was modeled as a 4 nm semispherical shell with a refractive index of 1.445,[31] under the hypothesis that the whole gold surface is covered by BSA molecules. Consequently, the longitudinal LSPR band was red-shifted by 4 nm, in good agreement with the experimental results (see Supporting Information Figure S3, red spectrum). Finally, we attempted on simulating the decoration of BSA-coated CTAB-AuNR with c-QDs. We point out that the c-QDs used in our experiments consist of CdSe/ZnS core−shell dots of approximately 3 nm radius[32] functionalized with sparse carboxylated polyethylene glycol chains. Considering the PEG-functionalized c-QDs as rigid spheres with radius of 6 nm,[33] the number of c-QDs bound to one BSA@CTAB-AuNR of 7500 nm^2 total area, as obtained for a 47 nm length and 22 nm width AuNR covered with 4 nm layers of CTAB and BSA, would be around 50 for a full coverage with closely packing spheres. However, in reality the loading capacity of BSA@CTAB-AuNR is much lower as proved by the TEM picture in Figure 2c where c-QDs are separated at distance above 6 nm, meaning less than 50 c-QDs per particle. Such corona of c-QDs can be modeled in the first approximation as a continuous layer of dielectric of 6 nm thickness with an effective refractive index of about 1.41 (volume weighted value calculated from the refractive indices of CdSe/ZnS core−shell dots and PEG layer, which are 2.433 and 1.465, respectively, under the supposition of ∼33% coverage inferred from TEM analysis). As a consequence, we have

dx.doi.org/10.1021/jp501281v | J. Phys. Chem. C 2014, 118, 25190−25199

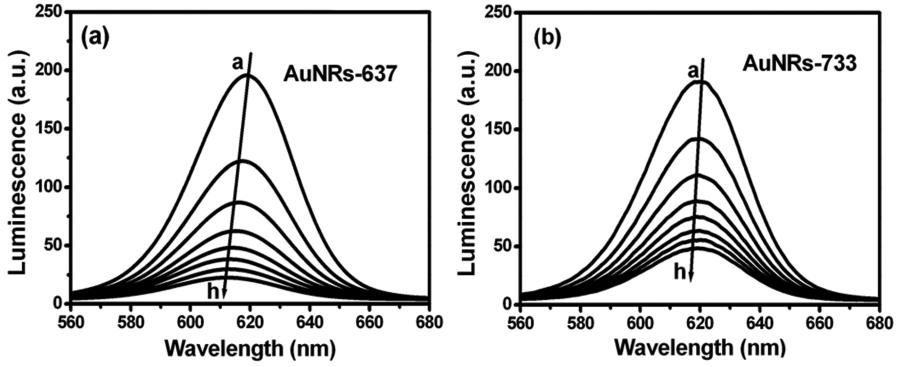

Figure 3. Evolution of luminescence spectra of c-QDs (2 nM) in the presence of increasing concentrations of (a) AuNRs-637 and (b) AuNRs-733, respectively. The nominal AuNRs concentrations from top to bottom are (a) 0, (b) 0.32×10^{-10} M, (c) 0.6×10^{-10} M, (d) 0.9×10^{-10} M, (e) 1.2×10^{-10} M, (f) 1.48×10^{-10} M, (g) 1.74×10^{-10} M, and (h) 2×10^{-10} M; $\lambda_{excitation}$ = 375 nm.

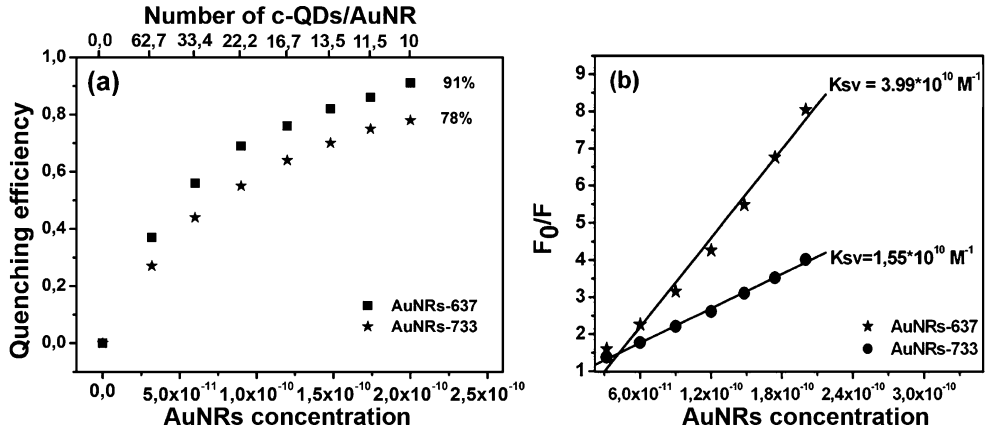

Figure 4. (a) Comparison of quenching efficiencies of AuNRs-637 and AuNRs-733; and (b) Stern–Volmer plots showing the luminescence quenching efficiencies of AuNRs-637 and AuNRs-733.

obtained an additional red-shift of 8 nm (see Supporting Information Figure S3, blue spectrum), rather close to the experimental value (see Supporting Information Figure S3).

Luminescence Quenching of c-QDs by AuNRs. The effect of conjugation of c-QDs to as-synthesized nanoparticles (i.e., AuNRs-637 and AuNRs-733) on the luminescence properties was systematically investigated by steady-state luminescence spectroscopy. It is worth mentioning that the luminescence spectrum of c-QDs was measured by using 375 nm as excitation wavelength, excluding in this case the excitation of metallic nanoparticles via its surface plasmon resonance, which occurs above 510 nm for AuNRs. Indeed, when a certain amount of c-QDs solution was mixed with CTAB-coated AuNRs solution, the luminescence intensity decreased rapidly together with a slight blue-shift of the luminescence maximum, as compared to reference sample of c-QDs in the absence of the AuNRs (see Figure 3). A control experiment has been carried out to evaluate the long-term stability of free c-QDs in PBS solution for up to 20 days and found no sign of luminescence quenching. This suggests that the c-QDs are not vulnerable to aggregation in the concentration range of 1–2 nM in PBS solution (see Supporting Information Figure S4). We then noticed interesting behavior of c-QDs luminescence when mixed with the CTAB molecules in water. For instance, at high CTAB concentration (10^{-4} M), c-QDs exhibit increased luminescence relative to low concentration and free c-QDs in pure water, which can be explained by the fact that CTAB molecules at high concentration form colloidal micelles, which in turn can engage the anionic c-QDs molecules and reduce the overall rate of nonradiative process. On the other hand, at low CTAB concentration, the luminescence decreases with respect to free c-QDs as in this case for c-QDs strongly interacting with cationic CTAB molecules the nonradiative deactivation increases (data not shown here).[34] It is therefore expected that similar quenching effect should contribute to overall quenching when c-QDs molecules bound to AuNRs via CTAB layer coating.

More precisely, Figure 3 shows the evolution of luminescence as result of mixing the same amount (2 nM) of c-QDs with increasing amounts of AuNRs (0.32×10^{-10} M; 0.6×10^{-10} M; 0.9×10^{-10} M; 1.2×10^{-10}; 1.48×10^{-10} M; 1.74×10^{-10} M; and 2×10^{-10} M), which provide 63 to 10 c-QDs per one metallic nanoparticle. Given the number of PEG-functionalized c-QD per metallic nanoparticle for full coverage (34:1, as calculated for a AuNR of 47 nm length and 22 nm width, covered with a 4 nm CTAB layer, and 6 nm radius PEG-functionalized c-QDs) and relatively large QDs–QDs distance (see Figure 2c), the interaction between loaded and free QDs can be considered negligible and not affecting the evolution of luminescence presented in Figure 3.

In our case, the variation of the quenching efficiency presented in Figure 3 originates from the degree of spectral overlap between the longitudinal LSPR band of the AuNRs and the luminescence band of the c-QDs. Experimentally, the

dx.doi.org/10.1021/jp501281v | J. Phys. Chem. C 2014, 118, 25190–25199

quenching efficiencies (QE) can be determined from the steady-state luminescence data:[35]

$$QE = 1 - \frac{I_i}{I_0} \quad (1)$$

where I_i is the integrated luminescence intensity of the donor in the presence of acceptor and I_0 is the integrated luminescence intensity of the donor alone.

As shown in Figure 4a, the direct interaction of negatively charged c-QDs with the positively charged AuNRs induces a strong quenching of c-QDs luminescence with different efficiency rate, ranging from 78% for AuNRs-733 to 91% for AuNRs-637, as the concentration of nanoparticles reaches 2×10^{-10} M.

Furthermore, the difference in luminescence quenching efficiency is also clearly shown by linear Stern−Volmer (SV) plots, as indicated in Figure 3b, and quantified by the following equation:[35]

$$\frac{F_0}{F_i} = 1 + K_{sv}[q] \quad (2)$$

where F_0 and F_i are the luminescence intensities in the absence and in the presence of different concentration of quencher; K_{sv} is the SV quenching constant; and q is the concentration of the quencher, respectively. The calculated values of K_{sv} from SV plots are presented in Table 1.

Table 1. Calculated Stern Volmer quenching constants (K_{sv})

AuNRs	K_{sv} (M^{-1})	SD[a]	R^b
AuNRs-637	3.99×10^{10}	0.326	0.992
AuNRs-733	1.55×10^{10}	0.057	0.998

[a]SD is the standard deviation of the K_{sv} values. [b]R is the correlation coefficient.

In general, the rate of energy transfer is strongly dependent on several factors, such as the distance (d) of separation between the donor and proximal and the extent of spectral overlap.[35] For example, Förster resonance energy transfer (FRET), ascribed to $1/d^6$ dependence, is currently explored as a crucial tool for investigating different biological phenomena involving energy transfer. Li et al. reported that the energy transfer efficiency of CdSe/ZnS QDs followed the FRET mechanism and that the highest quenching efficiency value was obtained for 80 nm sized acceptor gold nanospheres, due to increased spectral overlap of the plasmonic band with the luminescence band of QDs.[36]

Surface energy transfer (SET) model has been recently reported to investigate the quenching effects of QDs or dye molecules.[37−39] Reineck et al. determined, both theoretically and experimentally, the distance and wavelength dependence of the electromagnetic coupling between Au@SiO_2 core−shell nanoparticles and nearby fluorophores.[37] Strouse's group demonstrated that SET is able to measure intermolecular distances up to 50 nm, depending on the size of the metallic nanoparticles involved.[40,41] For SET model, the quenching is inversely proportional to the fourth power of the distance between particles in analogy to the six power distance dependence that governs FRET formalism. More recently, Samanta et al. demonstrated that the quenching of QDs fluorescence is due to an increase in the nonradiative decay rate that is induced by the presence of 30 nm AuNPs. They found that, unlike FRET, the energy transfer is inversely proportional to the 2.7th power of the distance between particles.[42]

Herein, the observed quenching efficiency is attributed to a combination of factors such as (i) the large extinction coefficient of AuNRs, (ii) the overlap between the luminescence band of the c-QDs and the longitudinal LSPR band of AuNRs, and (iii) the close vicinity between c-QDs and CTAB-coated AuNRs surface. Additionally, we assume that the quenching of c-QDs induced by CTAB might also contribute to overall quenching of c-QDs molecules bound to AuNRs via CTAB layer coating. It should be mentioned that, in general, the energy transfer is most efficient when the distance between donors and acceptors is in the 20−60 Å range.[36] This condition is also fulfilled in our system taking into consideration that the CTAB bilayer covering the AuNRs surface plays the role of spacer by fixing the c-QDs at about 4 nm far from the AuNRs surface. Similar quenching effects of dye molecules on gold nanoparticles have been previously reported by Reineck et al. when the distance is less than 5 nm,[37] which is in agreement with our observations.

Luminescence Enhancement of c-QDs by AuNRs. The resonant excitation of the surface plasmons of the metallic

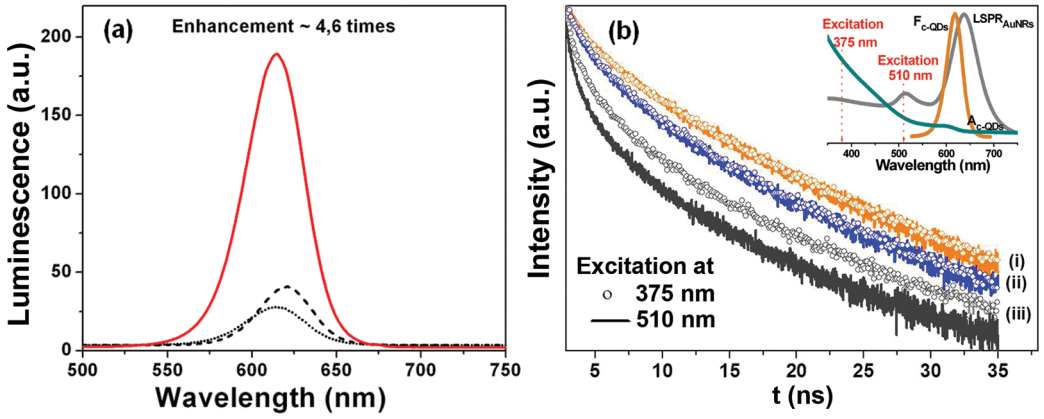

Figure 5. (a) Luminescence spectra of c-QDs (dashed spectrum), c-QDs@BSA system (dotted spectrum), and c-QDs decorated BSA@AuNRs-637 (red spectrum). $\lambda_{excitation}$ = 510 nm. (b) Normalized fluorescence lifetime decay curves of c-QDs (i), c-QDs decorated BSA@AuNRs-637 (ii), and c-QDs@AuNRs-637 (iii) obtained at $\lambda_{excitation}$ = 375 nm and $\lambda_{excitation}$ = 510 nm, respectively. Inset: Comparison between the position of the excitation wavelength and the optical response of AuNRs-637 and c-QDs.

dx.doi.org/10.1021/jp501281v | J. Phys. Chem. C 2014, 118, 25190−25199

Table 2. Decay Parameters of Free and Conjugated c-QDs

excitation (nm)	sample[a]	τ_1 [ns][b]	A_1 [%]	τ_2 [ns]	A_2 [%]	$\langle\tau\rangle$ [ns]	χ^{2c}
375	A	15.2 ± 0.1	60.5 ± 2	2.74 ± 0.07	39.5 ± 1.5	10.3	1.2
	B	13.35 ± 0.15	44 ± 1	2.1 ± 0.1	56 ± 1	7	1.5
	C	14 ± 0.1	52.5 ± 1.5	2.6 ± 0.03	47.5 ± 1.2	8.6	1.2
510	A	15.3 ± 0.3	60.5 ± 1.5	2.71 ± 0.08	39.5 ± 1.5	10.3	1.15
	B	11.35 ± 0.4	42 ± 1	1.57 ± 0.04	58 ± 1.5	5.7	1.2
	C	13.5 ± 0.3	53 ± 2.5	2.5 ± 0.06	47 ± 2	8.3	1.11

[a]A = c-QDs; B = c-QDs@AuNRs-637; C = c-QDs@BSA@AuNRs-637. [b]τ_n and A_n are lifetime and amplitude of the nth component; $\langle\tau\rangle$ is the amplitude-weighted average lifetime. [c]χ^2 indicates the goodness of the fit (1 corresponds to a perfect fit).

nanoparticles leads to the enhancement of the electromagnetic field at the nanoparticles surface, which can subsequently influence the luminescence rates of the molecules situated in their close proximity. We previously demonstrated that when c-QDs are directly adsorbed onto the CTAB-coated AuNR surface, the luminescence is quenched. The degree of quenching is depending on the spectral overlap between the longitudinal LSPR band of AuNRs and luminescence spectrum of c-QDs. However, it is known that at a distance of a few nanometers from the AuNR surface,[35] the luminescence of the QDs can be strongly enhanced by the means of several mechanisms, as the increase of excitation rate in the enhanced local electromagnetic field, increase of radiative lifetime of QDs by plasmon−exciton coupling in the near field, as well as by interaction of free space photons by scattering processes.

We note that the intensity of the c-QDs luminescence, located at 620 nm (Figure 5a, dashed spectrum), decreases while the band maximum blue-shifts with 5 nm after interaction of c-QDs with albumin (Figure 5a, dotted spectrum). This shift can be attributed to a change of the electronic structure of the c-QDs coated with protein.[43] Finally, when BSA protein acts as spacer layer to prevent the quenching mechanism, our c-QDs decorated BSA@AuNRs-637 system exhibits up to a 4.6-fold luminescence enhancement as compared to free c-QDs (Figure 5a, red spectrum) and a 39-fold luminescence enhancement relative to the corresponding case of c-QDs@AuNR system, under the excitation with the 510 nm wavelength. These enhanced values of the luminescence are attributed to the effect of local field excitation due to surface plasmon resonance. It is worth mentioning that all luminescence spectra were collected under identical excitation and detection conditions. On the contrary, under 375 nm excitation, we obtained 1.1-fold luminescence enhancement, as Supporting Information Figure S6 shows. This amplification factor is well correlated with the FDTD evaluation of the local field exhibited by AuNRs-637 at approximately 7−8 nm from the metal surface at 375 nm, where c-QDs are located, revealing an approximately 2.5-times smaller field at 375 nm as compared to 510 nm (Supporting Information Figure S5).

To get a better insight into the mechanisms involved in the enhancement of the luminescence of c-QDs when conjugated to BSA@AuNRs-637 and to confirm our previous findings, we investigated the changes in c-QDs excited-state lifetime and performed fluorescence lifetime measurements on free c-QDs and c-QDs conjugated to AuNRs-637 in the absence and presence of BSA. The decay curves, obtained for the three systems at the excitation of 375 and 510 nm, show two exponential components after deconvolution of the instrument response function (see Figure 5b). The decay fitting parameters are listed in Table 2.

The fluorescence lifetime of free c-QDs shows a biexponential behavior having an average value of 10.3 ns as calculated according to the formula:

$$\langle\tau\rangle = \frac{\sum \tau_i^* A_i}{\sum A_i} \tag{3}$$

where $\langle\tau\rangle$ is the average fluorescence lifetime and τ_i and A_i represent the decay time and amplitude, respectively, of each component (see Table 2). The measured lifetime corresponds well to the previously reported value.[44] At 510 nm excitation, in the presence of AuNRs-637, the average fluorescence lifetime of c-QDs strongly decreases to 5.7 ns as compared to 10.3 ns corresponding to the free c-QDs. The shortening of the lifetime of c-QDs confirms the efficient energy transfer[45] in our donor−acceptor system, in accordance with the previous results obtained on the quenching of the luminescence intensity from our steady-state fluorescence measurements. Specifically, the significant overlap between the emission of the c-QDs and the plasmon resonance of AuNRs-637 (see inset of Figure 5b) favors a resonance energy transfer from c-QDs to AuNRs-637. Additionally, the <5 nm layer of CTAB[30] stabilizing the AuNRs-637 promotes a strong interaction between c-QDs and the metallic surface, thus supporting the quenching of c-QDs fluorescence by AuNRs-637 via nonradiative energy transfer. As previously demonstrated, the larger is the overlapping between the longitudinal LSPR and the emission bands, the greater is the quenching. Thus, the significant decrease of the excited-state lifetime is well correlated with the results obtained from steady-state fluorescence measurements. On the contrary, under excitation at 375 nm, out of the plasmon resonances of AuNRs we obtain a value of 7 ns.

Furthermore, we have focused on the c-QDs decorated BSA@AuNRs-637 system with enhanced fluorescence properties, and we have investigated the excited-state lifetime under the same excitation at 510 nm. As illustrated in Figure 5b, curve ii, the decay curve displays a slight decrease as compared to bare c-QDs, the average lifetime being calculated at 8.3 ns. In this case, the presence of a BSA shell around AuNRs-637 surface helps in preventing the process of energy transfer from c-QDs to Au surface, which was already mentioned as being the dominating quenching effect. A similar behavior has been reported in an early paper of Medintz et al., who developed a FRET-based prototype QDs sensor assembly.[46] They have shown that overcoming the FRET mechanism between the QDs as donor and a fusion protein as acceptor results in a significant recovery of the donor lifetime. Additionally, we assume a competition between the decrease of the nonradiative decay rate due to a possible intercalation of c-QDs in the BSA layer and the increase of the radiative decay rate as a consequence of the matching of plasmon band with the luminescence of c-QDs.

dx.doi.org/10.1021/jp501281v | J. Phys. Chem. C 2014, 118, 25190−25199

Subsequently, we were interested in investigating the energy transfer between c-QDs and AuNRs-637 in the absence and presence of BSA because it is known that the nonradiative energy transfer between two dipoles is related to the donor−acceptor (here c-QDs−AuNR) separation, as we have previously discussed. The general formula known to describe this dependence is[47]

$$E = \frac{1}{1 + (d/d_0)^p} \tag{4}$$

where E is the nonradiative energy transfer, d is the separation between the donor and the acceptor, d_0 is the separation at which the energy transfer efficiency is 50%, and p is dependent on the mechanism of energy transfer from the donor to the acceptor. In FRET mechanism, $p = 6$, while d_{0FRET} can be described as[48]

$$d_{0FRET} = 0.211[k^2 \Phi_0 n^{-4} J(\lambda)]^{1/6} \tag{5}$$

where k^2 describes the relative orientation in space of the transition dipoles of the donor and the acceptor and is taken to be 2/3 assuming rapid orientational averaging of the donor within the lifetime of its excited state, Φ_0 is the quantum yield of donor fluorescence without acceptor (here 0.77 for 620 nm emitting c-QDs), n is the refractive index of the medium (here 1.426, corresponding to the volume weighted value of CTAB and BSA layers employed in the FDTD simulations), and $J(\lambda)$ is the overlap integral between the normalized donor emission and the acceptor extinction coefficient, expressed as follows:

$$J(\lambda) = \int_0^\infty F_D(\lambda)\varepsilon_A(\lambda)\lambda^4 \, d\lambda \tag{6}$$

where $F_D(\lambda)$ is the fluorescence intensity of the donor in the absence of acceptor (the integral of the spectrum equals one), and $\varepsilon_A(\lambda)$ is the wavelength-dependent molar extinction coefficient of the acceptor. For the SET mechanism, $p = 4$, and d_{0SET} can be obtained with[49]

$$d_{0SET} = \left[0.225 \frac{\Phi_{c\text{-}QDs}}{\omega_{c\text{-}QDs}^2} \frac{1}{\omega_F k_F} \frac{c^3}{n}\right]^{1/4} \tag{7}$$

where c is the speed of light in a vacuum, n is the refractive index of the medium (1.426), $\Phi_{c\text{-}QDs}$ is the fluorescence quantum yield of donor, here c-QDs, $\omega_{c\text{-}QDs}$ is the angular frequency for the donor (3.04×10^{15} s^{-1} for 620 nm emitting c-QDs), while ω_F and k_F represent the angular frequency of the metal (8.4×10^{15} s^{-1}, bulk gold) and the Fermi wave vector of metal (1.2×10^8 cm^{-1}, bulk gold), respectively.

To understand the origin of the energy transfer between c-QDs and AuNRs, we have plotted the theoretical energy transfer efficiency curves based on FRET and SET mechanisms (see Figure 6) along with the FDTD simulated quenching efficiencies at different separation distances between c-QDs and the metal surface of AuNRs with LSPR at 637 nm, respectively.

In FDTD simulations, we considered the emitting c-QD as an oscillating dipole radiating in the interval 530−690 nm, placed at different distances from a 47 × 22 nm AuNR exhibiting longitudinal LSPR at 637 nm (AuNR-637), along its short axis and polarized along its longitudinal axis. The nonradiative rates were calculated for distances d between 2 and 18 nm and normalized with respect to the free space case. The value of the overlap integral in our case was found to be 3.2×10^{20} M^{-1} cm^{-1} nm^4, while for d_{0FRET} and d_{0SET} we found

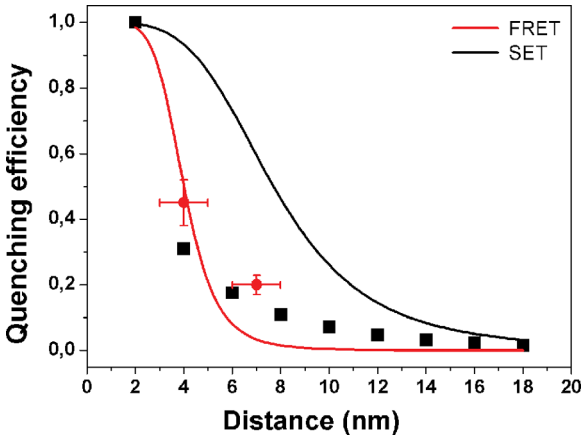

Figure 6. Simulated data points of the quenching efficiency at different separation distances between c-QDs and AuNR-637 (■) metal surface, along with the experimental data points obtained for c-QDs conjugated to AuNRs-637 in the presence and absence of BSA (red ●) and theoretical curves of the quenching efficiency based on the FRET (red curve) and SET (black curve) models.

4 and 7.7 nm, respectively. To elucidate the quenching mechanism in our system, we have investigated the position of the experimental quenching efficiencies obtained for c-QDs conjugated to AuNRs in the presence and the absence of BSA relative to the theoretical curves of the quenching efficiency based on the FRET and SET models (see Figure 6). We first calculated the quenching efficiencies (QE) of c-QDs coupled to AuNRs-637 and BSA@AuNRs-637 according to the formula:

$$QE = 1 - \frac{\tau}{\tau_0} \tag{8}$$

where τ_0 represents the lifetime of free c-QDs (10.3 ns) and τ represents the lifetime of c-QDs@AuNR-637 (5.7 ns) and c-QDs@BSA@AuNRs-637 (8.3 ns), as presented in Table 2.

Figure 6 demonstrates that the FRET model provides a better fit to the experimental data, this result being expected considering the spectral overlap between the luminescence of c-QDs and the longitudinal LSPR band of AuNRs-637.

■ CONCLUSIONS

In summary, the quenching mechanism between c-QDs and AuNRs of different aspect ratios in aqueous solution was first investigated. We found that the luminescence quenching efficiency depends on the spectral overlap between the luminescence of c-QDs and the longitudinal LSPR band. Thus, the highest quenching efficiency was obtained for the AuNRs with the longitudinal LSPR located at 637 nm, best overlapping the luminescence band of c-QDs. Additionally, the shortening of the excited-state lifetime of c-QDs in the presence of AuNPs-637 sustains the hypothesis of the energy transfer. We have demonstrated that the quenching of the luminescence of c-QDs can be successfully avoided by coating the AuNRs-637 with BSA protein prior to decoration with c-QDs by excitation of metallic nanoparticles via its surface plasmon resonance, which occurs above 510 nm for AuNRs. The experimental LSPR response of AuNRs in the presence of BSA and c-QDs molecules was confirmed at the theoretical level by FDTD calculations. By playing the role of both linker and spacer for keeping the c-QDs at a favorable distance from the AuNRs, BSA triggers a 4.6-fold enhancement of the luminescence of free c-QDs and a 39-fold luminescence

dx.doi.org/10.1021/jp501281v | J. Phys. Chem. C 2014, 118, 25190−25199

enhancement relative to the corresponding case of c-QDs@AuNR system. The interaction of c-QDs with AuNRs in the presence and absence of BSA was also investigated through time-resolved florescence spectroscopy, further confirming the involvement of FRET mechanism and protective role of BSA layer. In conclusion, AuNRs offer excellent potential to modify electromagnetic field, enabling the design of new metallic nanoantennas−QDs complexes with appealing luminescence properties for further development of significant biological applications.

■ ASSOCIATED CONTENT

Supporting Information

IRF temporal profile, TEM images, comparison of longitudinal plasmon resonance bands, stability of free c-QDs in PBS, map of the electric field intensity, and luminescence spectra. This material is available free of charge via the Internet at http://pubs.acs.org.

■ AUTHOR INFORMATION

Corresponding Author

*Tel: +40 264 405300/5188. Fax: +40 264 591906. E-mail: simion.astilean@phys.ubbcluj.ro.

Notes

The authors declare no competing financial interest.

■ ACKNOWLEDGMENTS

This work was supported by CNCS − UEFISCDI Romania, under the project number PNII-ID-PCCE-0069/2011. M.F. gratefully acknowledges the financial support from the Babes-Bolyai University, project number GTC_34022/2013.

■ REFERENCES

(1) Li, X.; Qian, J.; Jiang, L.; He, S. Fluorescence Quenching of Quantum Dots by Gold Nanorods and its Application to DNA Detection. *Appl. Phys. Lett.* **2009**, *94*, 063111.
(2) Qi, L.; Gao, X. Quantum Dot−Amphipol Nanocomplex for Intracellular Delivery and Real-Time Imaging of siRNA. *ACS Nano* **2008**, *2*, 1403−1410.
(3) Schuck, P. J.; Fromm, D. P.; Sundaramurthy, A.; Kino, G. S.; Moerner, W. E. Improving the Mismatch between Light and Nanoscale Objects with Gold Bowtie Nanoantennas. *Phys. Rev. Lett.* **2005**, *94*, 017402.
(4) Chen, H. Y.; Lo, M. K. F.; Yang, G.; Monbouquette, H. G.; Yang, Y. Nanoparticle-Assisted High Photoconductive Gain in Composites of Polymer and Fullerene. *Nat. Nanotechnol.* **2008**, *3*, 543−547.
(5) Okamoto, K.; Vyawahare, S.; Scherer, A. Surface-Plasmon Enhanced Bright Emission from CdSe Quantum-Dot Nanocrystals. *J. Opt. Soc. Am. B* **2006**, *23*, 1674−1678.
(6) Huang, F. M.; Festy, F.; Richards, D. Tip-Enhanced Fluorescence Imaging of Quantum Dots. *Appl. Phys. Lett.* **2005**, *87*, 183101.
(7) Aldeek, F.; Ji, X.; Mattoussi, H. Quenching of Quantum Dot Emission by Fluorescent Gold Clusters: What It Does and Does Not Share with the Förster Formalism. *J. Phys. Chem. C* **2013**, *117*, 15429−15437.
(8) Lakowicz, J. R.; Shen, Y.; D'Auria, S.; Malicka, J.; Fang, J.; Gryczynski, Z.; Gryczynski, I. Radiative Decay Engineering 2. Effects of Silver Island Films on Fluorescence Intensity, Lifetimes, and Resonance Energy Transfer. *Anal. Biochem.* **2002**, *301*, 261−277.
(9) Haridas, M.; Basu, J. K.; Tiwari, A. K.; Venkatapathi, M. Photoluminescence Decay Rate Engineering of CdSe Quantum Dots on Ensemble Arrays Embedded with Gold Nano-Antennae. *J. Appl. Phys.* **2013**, *114*, 064305.
(10) Griffin, J.; Singh, A. K.; Senapati, D.; Rhodes, P.; Mitchell, K.; Robinson, B.; Yu, E.; Ray, P. C. Size- and Distance-Dependent Nanoparticle Surface-Energy Transfer (NSET) Method for Selective Sensing of Hepatitis C Virus RNA. *Chem.—Eur. J.* **2009**, *15*, 342−351.
(11) Kulakovich, O.; Strekal, N.; Yaroshevich, A.; Maskevich, S.; Gaponenko, S.; Nabiev, I.; Woggon, U.; Artemyev, M. Enhanced Luminescence of CdSe Quantum Dots on Gold Colloids. *Nano Lett.* **2002**, *2*, 1449−1452.
(12) Liu, N.; Prall, B. S.; Klimov, V. I. Hybrid Gold/Silica/Nanocrystal-Quantum-Dot Superstructures: Synthesis and Analysis of Semiconductor−Metal Interactions. *J. Am. Chem. Soc.* **2006**, *128*, 15362−15363.
(13) Lee, J.; Govorov, A. O.; Dulka, J.; Kotov, N. A. Bioconjugates of CdTe Nanowires and Au Nanoparticles: Plasmon−Exciton Interactions, Luminescence Enhancement, and Collective Effects. *Nano Lett.* **2004**, *4*, 2323−2330.
(14) Freddi, S.; D'Alfonso, L.; Collini, M.; Caccia, M.; Sironi, L.; Tallarida, G.; Caprioli, S.; Chirico, G. Excited-State Lifetime Assay for Protein Detection on Gold Colloids−Fluorophore Complexes. *J. Phys. Chem. C* **2009**, *113*, 2722−2730.
(15) Lee, J.; Javed, T.; Skeini, T.; Govorov, A. O.; Bryant, G. W.; Kotov, N. A. Bioconjugated Ag Nanoparticles and CdTe Nanowires: Metamaterials with Field-Enhanced Light Absorption. *Angew. Chem., Int. Ed.* **2006**, *45*, 4819−4823.
(16) Kinkhabwala, A.; Yu, Z.; Fan, S.; Avlasevich, Y.; Mullen, K.; Moerner, W. E. Large Single-Molecule Fluorescence Enhancements Produced by a Bowtie Nanoantenna. *Nat. Photonics* **2009**, *3*, 654−657.
(17) Stockman, M. I. Spaser Action, Loss Compensation, and Stability in Plasmonic Systems with Gain. *Phys. Rev. Lett.* **2011**, *106*, 156802.
(18) Zhang, J.; Fu, Y.; Chowdhury, M. H.; Lakowicz, J. R. Enhanced Förster Resonance Energy Transfer on Single Metal Particle. 2. Dependence on Donor−Acceptor Separation Distance, Particle Size, and Distance from Metal Surface. *J. Phys. Chem. C* **2007**, *111*, 11784−11792.
(19) Nikoobakht, B.; El-Sayed, M. A. Preparation and Growth Mechanism of Gold Nanorods (NRs) Using Seed-Mediated Growth Method. *Chem. Mater.* **2003**, *15*, 1957−1962.
(20) Amundson, K.; Helfand, E.; Patel, S. S.; Quan, X.; Smith, S. D. Optical Characterization of Ordering and Disordering of Block Copolymer Microstructure. *Macromolecules* **1992**, *25*, 1935−1940.
(21) Iosin, M.; Toderas, F.; Baldeck, P. L.; Astilean, S. Study of Protein-Gold Nanoparticles Conjugates by Fluorescence and Surface-Enhanced Raman Scattering. *J. Mol. Struct.* **2009**, *924−926*, 196−200.
(22) Cottat, M.; Thioune, N.; Gabudean, A. M.; Lidgi-Guigui, N.; Focsan, M.; Astilean, S.; Lamy de la Chapelle, M. Localized Surface Plasmon Resonance (LSPR) Biosensor for the Protein Detection. *Plasmonics* **2013**, *8*, 699−704.
(23) Thioune, N.; Lidgi-Guigui, N.; Cottat, M.; Gabudean, A. M.; Focsan, M.; Benoist, G. M.; Astilean, S.; Lamy de la Chapelle, M. Study of Gold Nanorods−Protein Interaction by Localized Surface Plasmon Resonance Spectroscopy. *Gold Bull.* **2013**, *46*, 275−281.
(24) Orendorff, C. J.; Murphy, C. J. Quantitation of Metal Content in the Silver-Assisted Growth of Gold Nanorods. *J. Phys. Chem. B* **2006**, *110*, 3990−3994.
(25) Potara, M.; Gabudean, A. M.; Astilean, S. Solution-Phase, Dual LSPR-SERS Plasmonic Sensors of High Sensitivity and Stability Based on Chitosan-Coated Anisotropic Silver Nanoparticles. *J. Mater. Chem.* **2011**, *21*, 3625−3633.
(26) Sivakumar, R. N.; Anandan, S. Interactions of Serum Albumins with Antitumor Agent Benzo [A] Phenazine - A Spectroscopic Study. *J. Lumin.* **2011**, *131*, 2195−2201.
(27) Zhang, D.; Neumann, O.; Wang, H.; Yuwono, V. M.; Barhoumi, A.; Perham, M.; Hartgerink, J. D.; Wittung-Stafshede, P.; Halas, N. J. Gold Nanoparticles Can Induce the Formation of Protein-based Aggregates at Physiological pH. *Nano Lett.* **2009**, *9*, 666−671.
(28) www.lumerical.com/fdtd.php.
(29) Johnson, P. B.; Christy, R. W. Optical Constants of the Noble Metals. *Phys. Rev. B* **1972**, *6*, 4370−4379.

(30) Yu, C.; Varghese, L.; Irudayaraj, J. Surface Modification of Cetyltrimethylammonium Bromide-Capped Gold Nanorods to Make Molecular Probes. *Langmuir* **2007**, *23*, 9114−9119.
(31) Tsargorodskaya, A.; Nabok, A. V.; Ray, A. K. Ellipsometric Study of The Adsorption Of Bovine Serum Albumin into Porous Silicon. *Nanotechnology* **2004**, *15*, 703.
(32) Pelossof, G.; Tel-Vered, R.; Liu, X.; Willer, I. Switchable Mechanical DNA "Arms" Operating on Nucleic Acid Scaffolds Associated with Electrodes or Semiconductor Quantum Dots. *Nanoscale* **2013**, *5*, 8977−8981.
(33) Kelf, T. A.; Sreenivasan, V. K. A.; Sun, J.; Kim, E. J.; Goldys, E. M.; Zvyagin, A. V. Non-Specific Cellular Uptake of Surface-Functionalized Quantum Dots. *Nanotechnology* **2010**, *21*, 285105.
(34) Bilski, P.; Dabestani, R.; Chignell, C. F. Influence of Cationic Surfactant on the Photoprocesses of Eosine and Rose Bengal in Aqueous Solution. *J. Phys. Chem.* **1991**, *95*, 5784−5791.
(35) Lakowicz, J. R. *Principles of Fluorescence Spectroscopy*; Kluwer Academic/Plenum Publishers: New York, 1999.
(36) Li, M.; Cushing, S. K.; Wang, Q.; Shi, X.; Hornak, L. A.; Hong, Z.; Wu, N. Size-Dependent Energy Transfer between CdSe/ZnS Quantum Dots and Gold Nanoparticles. *J. Phys. Chem. Lett.* **2011**, *2*, 2125−2129.
(37) Reineck, P.; Gómez, D.; Ng, S. H.; Karg, M.; Bell, T.; Mulvaney, P.; Bach, U. Distance and Wavelength Dependent Quenching of Molecular Fluorescence by Au@SiO2 Core−Shell Nanoparticles. *ACS Nano* **2013**, *7*, 6636−6648.
(38) Acuna, G. P.; Bucher, M.; Stein, I. H.; Steinhauer, C.; Kuzyk, A.; Holzmeister, P.; Schreiber, R.; Moroz, A.; Stefani, F. D.; Liedl, T.; et al. Distance Dependence of Single-Fluorophore Quenching by Gold Nanoparticles Studied on DNA Origami. *ACS Nano* **2012**, *6*, 3189−3195.
(39) Griffin, J.; Singh, A. K.; Senapati, D.; Rhodes, P.; Mitchell, K.; Robinson, B.; Yu, E.; Ray, P. C. Size- and Distance-Dependent Nanoparticle Surface-Energy Transfer (NSET) Method for Selective Sensing of Hepatitis C Virus RNA. *Chem.—Eur. J.* **2009**, *15*, 342−351.
(40) Breshike, C. J.; Riskowski, R. A.; Strouse, G. F. Leaving Förster Resonance Energy Transfer Behind: Nanometal Surface Energy Transfer Predicts the Size-Enhanced Energy Coupling between a Metal Nanoparticle and an Emitting Dipole. *J. Phys. Chem. C* **2013**, *117*, 23942−23949.
(41) Jennings, T. L.; Singh, M. P.; Strouse, G. F. Fluorescent Lifetime Quenching near d =1.5 nm Gold Nanoparticles: Probing NSET Validity. *J. Am. Chem. Soc.* **2006**, *128*, 5462−5467.
(42) Anirban, S.; Yadong, Z.; Shengli, Z.; Han, Y.; Yan, L. Fluorescence Quenching of Quantum Dots by Gold Nanoparticles: A Potential Long Range Spectroscopic Ruler. *Nano Lett.* **2014**, *14*, 5052−5057.
(43) Dif, A. l.; Henry, E.; Artzner, F.; Baudy-Floch, M. l.; Schmutz, M.; Dahan, M.; Marchi-Artzner, V. R. Interaction between Water-Soluble Peptidic CdSe/ZnS Nanocrystals and Membranes: Formation of Hybrid Vesicles and Condensed Lamellar Phases. *J. Am. Chem. Soc.* **2008**, *130*, 8289−8296.
(44) van Sark, W. G. J. H. M.; Frederix, P. L. T. M.; Bol, A. A.; Gerritsen, H. C.; Meijerink, A. Blueing, Bleaching, and Blinking of Single CdSe/ZnS Quantum Dots. *ChemPhysChem* **2002**, *3*, 871−879.
(45) Shivkumar, M. A.; Inamdar, L. S.; Rabinal, M. H. K.; Mulimani, B. G.; Rao, G. M. A; Inamdar, S. R. FRET from CdSe/ZnS Core-Shell Quantum Dots to Fluorescein 27 Dye. *Open J. Phys. Chem.* **2013**, *3*, 40−48.
(46) Medintz, I. L.; Clapp, A. R.; Mattoussi, H.; Goldman, E. R.; Fisher, B.; Mauro, J. M. Self-Assembled Nanoscale Biosensors Based on Quantum Dot FRET Donors. *Nat. Mater.* **2003**, *2*, 630−638.
(47) Singh, M. P.; Strouse, G. F. Involvement of the LSPR Spectral Overlap for Energy Transfer Between a Dye and Au Nanoparticle. *J. Am. Chem. Soc.* **2010**, *132*, 9383−9391.
(48) Lakowicz, J. R. *Principles of Fluorescence Spectroscopy*, 3rd ed.; Springer Academic: New York, 2006.
(49) Zhang, X.; Marocico, C. A.; Lunz, M.; Gerard, V. A.; Gunko, Y. K.; Lesnyak, V.; Gaponik, N.; Susha, A. S.; Rogach, A. L.; Bradley, A. L. Wavelength, Concentration, and Distance Dependence of Non-radiative Energy Transfer to a Plane of Gold Nanoparticles. *ACS Nano* **2012**, *10*, 9283−9290.